8,8′-Bi(8-azabicyclo[3.2.1]octane) and Its Oxidized Forms

Stephen F. Nelsen,*[1a] Glen T. Cunkle,[1a] Dennis H. Evans,[1a] Kenneth J. Haller,[1a] Menahem Kaftory,[1b] Burkhard Kirste,[1c] Harry Kurreck,[1c] and Timothy Clark[1d]

Contribution from the Department of Chemistry, S. M. McElvain Laboratories of Organic Chemistry, University of Wisconsin, Madison, Wisconsin 53706, Department of Chemistry, Israel Institute of Tecnology, Technion City, Haifa 32000, Israel, the Institut fur Organische Chemie, Freie Universität Berlin, 1000 Berlin 33, Federal Republic of Germany, and the Institut für Organische Chemie der Friedrich-Alexander-Universität, Erlangen-Nürnberg, D-8520 Erlangen, Federal Republic of Germany. *Received October 1, 1984*

Abstract: The crystal structure of 8,8′-bi(8-azabicyclo[3.2.1]octane, **1**, shows it to exist in the anti-AA conformation in the solid, as does its radical carbon nitrate salt $\mathbf{1}^+NO_3^-H_2O$. The bond length shortens 1.469 (2) to 1.323 (4) Å, and the average of the bond angles at nitrogen increases from 107.9° to 115.6° upon electron removal. ^{13}C NMR studies show that neutral **1** is most stable in the anti-EE conformation in solution, with the syn-AE/EA conformations 0.2_5 kcal/mol higher in energy and the anti-AA conformation another 0.2_5 kcal/mol higher in energy at −70 °C in methylene chloride. The average barrier separating these conformations is 12.3 kcal/mol. ENDOR experiments show that $\mathbf{1}^+$ is also in the anti-AA conformation in solution, although it is probably substantially flatter at nitrogen than it is in the crystal. *syn*-$\mathbf{1}^+$ is shown by CV studies to be 1.4_5 ($\pm 0.1_5$) kcal/mol less stable than is *anti*-$\mathbf{1}^+$ at 22 °C in acetonitrile containing 0.14 M tetra-*n*-butylammonium perchlorate. The wavelength maximum for UV absorption of $\mathbf{a1}^+$ is 337 nm, $\mathbf{s1}^+$, 318 nm. $\Delta G^{\ddagger}$ for thermal conversion of $\mathbf{s1}^+$ to $\mathbf{a1}^+$ was determined to be 22.0 kcal/mol at 25 °C from a combination of CV and UV measurements of the barrier which covered a temperature range from +6 to +41 °C. The second-order rate constant for the reaction $\mathbf{s1}^+ + \mathbf{a1}^0 \rightarrow \mathbf{a1}^+ + \mathbf{s1}^0$ was determined to be 4500 M^{-1} s^{-1} at 22 °C (reverse reaction, 260 M^{-1} s^{-1}) from a combination of CV and UV measurements. MNDO calculations are surprisingly successful at giving the geometries for $\mathbf{1}^+$.

The hydrazine–hydrazine radical cation electron transfer shown in eq 1 shows unusual characteristics. The thermodynamics for the I, I^+ equilibrium are not dominated by the energy of the highest occupied molecular orbital, homogeneous electron transfer between

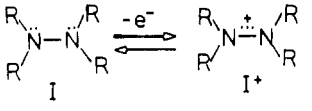

(1)

I and I^+ is far slower than for other $\Delta G = 0$ electron transfers in organic systems, and the heterogeneous rate constant for oxidation of I is strongly dependent upon the lone pair, lone pair dihedral angle θ[2]. Because the lone pairs of I interact (the splitting between the orbitals dominated by the bonding and antibonding lone pair combinations varies between about 0.5 eV when θ is near 90° and about 2.3 eV when θ is near 180° or 0°), the electron removed in going to the $3e^-$ π-bonded species I^+ is significantly antibonding. The effect of R groups on the thermodynamics for electron transfer clearly shows that the nitrogens flatten upon electron removal and that the NN bond rotational preference changes from perpendicular ($\theta = 90°$) in neutral I to a stronger preference for copolanar lone pairs ($\theta = 180°$ or 0°) in I^+. The unusual electron transfer characteristics for I, I^+ have been attributed to an unusually large geometry change between the two oxidation forms.[2]

As pointed out in the communication,[3] work in the 8,8′-bi(8-azabicyclo[3.2.1]octane), **1**, system has provided the first quantitative measure of the strength of the $3e^-$ π bond of I^+. The dissymetry of the R_2N groups of **1** causes the two isomeric forms of $\mathbf{1}^+$ (those with like bridges syn and anti) to be interconvertable by NN bond rotation, which requires breaking the $3e^-$ π bond.

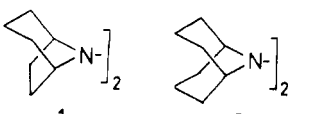

1 2

Analysis of the $\mathbf{s1}^+/\mathbf{a1}^+$ ratio could be accomplished by cyclic voltammetry, because these species oxidize at significantly different potentials. The kinetic stabilization of the oxidized forms of **1** provided by the $C_\alpha H$ bonds of its R_2N groups being held close to the nodal plane of the charge-bearing p orbital at nitrogen was necessary for this analysis and was predictable from the behavior of the previously studied[4] 9,9′-bi(9-azabicyclo[3.3.1]nonane) system, **2**. We were unable to successfully predict which $\mathbf{1}^+$ isomer was the most stable, because we had no idea why the $\mathbf{1}^+$ isomer formed at lowest oxidation potential is the most difficult to oxidize to the dication.[3] In this work, the size of the geometry change between crystalline **1** and $\mathbf{1}^+$ is quantitatively determined by X-ray crystallography and compared with the less quantitative information on solution conformations of these species from magnetic resonance experiments, and the turn-around in thermodynamic stability of the $\mathbf{1}^+$ and $\mathbf{1}^{2+}$ isomers is considered by using MNDO calculations for these species. The rotational barrier for $\mathbf{1}^+$ has been determined by cyclic voltammetry and UV spectroscopy, and the barriers to electron transfer between **1** and $\mathbf{1}^+$ have been determined by using both CV and UV.

Results and Discussion

1. Crystal Structure of 1. Isolation of **1** (apparently as an oil) has been reported by Mann and co-workers[5] from the electrochemical oxidation of nortropane (8-azabicyclo[3.2.1]octane). We prepared it by a method analogous to that previously reported for **2** (see Experimental Section). As expected from the structure of **2**, **1** has the nitrogen lone pairs anti to each other (lone pair, lone pair dihedral angle $\theta = 180°$), and as can be seen from the thermal ellipsoid plot (Figure 1), **1** is in the anti-AA conformation. In labeling the conformations, syn and anti refer to the orientation of like bridges (i.e., $(CH_2)_3$ or $(CH_2)_2$) of the bicyclic skeleton while A and E denote whether the $N-NR_2$ bond is axial or equatorial to the piperidine ring. The bond lengths and angles for **1** are shown in Figure 2, and tables including dihedral angles are given in the supplementary material. Those of the bicyclic

(1) (a) University of Wisconsin. (b) Israel Institute of Technology. (c) Freie Universität, Berlin. (d) Friedrich-Alexander-Universität, Erlangen-Nürnberg.

(2) Nelsen, S. F. *Acc. Chem. Res.* **1981**, *14*, 131.

(3) Nelsen, S. F.; Cunkle, G. T.; Evans, D. H.; Clark, T. *J. Am. Chem. Soc.* **1983**, *105*, 5928.

(4) (a) Nelsen, S. F.; Hollinsed, W. C.; Kessel, C. R.; Calabrese, J. C. *J. Am. Chem. Soc.* **1978**, *100*, 7876. (b) Nelsen, S. F.; Kessel, C. R.; Brien, D. J. *J. Am. Chem. Soc.* **1980**, *102*, 702.

(5) Laube, B. L.; Asirvatham, M. R.; Mann, C. J. *J. Org. Chem.* **1977**, *42*, 670.

0002-7863/85/1507-3829$01.50/0

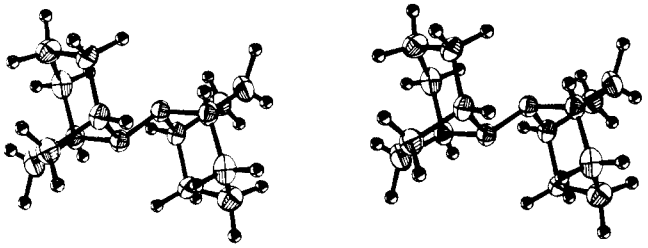

Figure 1. Stereoview of 1.

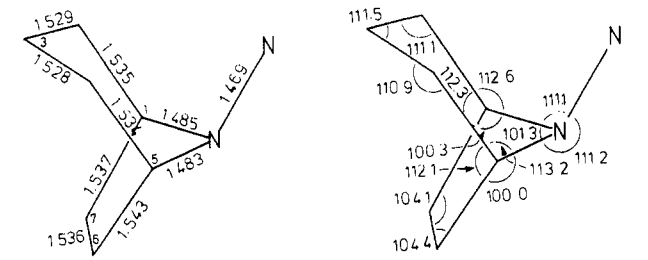

Figure 2. Bond lengths (Å) and bond angles (deg) for 1 (see Tables VI and VII for errors).

framework are quite similar to those of crystalline pseudotropine (3)[6] and even closer to those calculated by Allinger's MM2

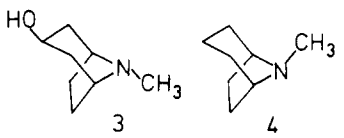

3 4

method[7] for axial 8-methyl-8-azabicyclo[3.2.1]octane, 4, demonstrating once more the value of molecular mechanics for accurate estimation of geometries.

The NN bond length observed for 1 (1.469 (2) Å) is 0.036 Å shorter than that of 2 (1.505 (3) Å), although both have $\theta = 180°$. The average of the bond angles at nitrogen is 107.9° for 1 and 108.3° for 2, so the pyramidality at nitrogen is rather similar for these species. The CNC angle is smaller in 1 than in 2 by 5.4°, but the angle the NN bond makes with the CNC plane, β_{NN}, is 55.3° for 1, 1.6° less than that of 2. MNDO calculations[8] on H_2NNH_2 held at $\theta = 180°$, varying the pyramidality at N and the HNH angle, do predict a shortening of the NN bond as the HNH angle is decreased, but the predicted change is on the order of a tenth as large as the observed d_{NN} difference. The fact that MNDO gets the NN distance of hydrazine much too short (less than 1.40 Å, compared with the actual value of 1.45 Å) and produces the minimum energy at $\theta = 180°$ instead of near $\theta = 90°$ gives us little confidence in the ability of MNDO calculations to deal property with geometry changes upon lone pair rehybridization in neutral hydrazines. It appears that hydrazine NN bond lengths are quite sensitive to the bond angles at nitrogen as well as the lone pair, lone pair dihedral angle, but too few data are presently available to evalute the effects quantitatively.

2. Crystal Structure of 1^+. 1^+ salts proved isolably stable, as expected from our work on 2^+ salts. We first attempted a crystal structure of $1^+PF_6^-$, but its crystals proved to be disordered with respect to the $(CH_2)_3$ and $(CH_2)_2$ bridges. Hoping that better differentiation between them would be achieved by having a smaller and less symmetrical conterion, we chose the nitrate salt, which was prepared by reaction with $AgNO_3$. These crystals were not disordered at the organic cation, although they proved to have a water of solvation and to be disordered at the NO_3^- anion. Figure 3 shows the thermal ellipsoid plot for 1^+, which proves to be in the anti-AA conformation. The bond lengths and angles are shown in Figure 4, and tables including dihedral angles appear in the supplementary material. Cyclic voltammetry studies showed that both the hexafluorophosphate and nitrate salts are in anti conformations.

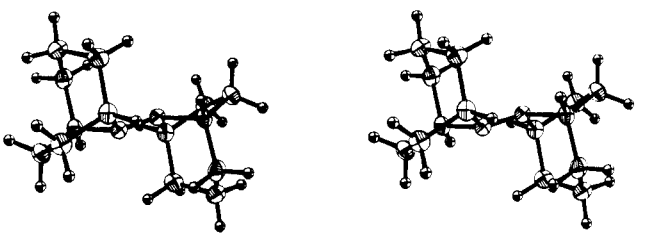

Figure 3. Stereoview of 1^+.

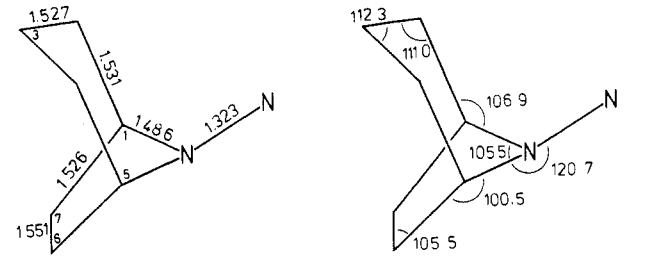

Figure 4. Bond length (Å) and bond angles (deg) for 1^+NO_2 (see Tables VI and VII for errors and information on the nitrate group).

The structure of 1^+ does not agree well at all with that reported for $2^+PF_6^-$.[4a] The 2^+ NN distance was 0.054 Å shorter than that of 1^+, and the NN bond, CNC plane angle β(NN) of 2^+ was 0°, while 1^+ is significantly bent, β(NN) = 32.5°. As previously noted, the NN distance found for 2^+ was anomalously short, and the crystal had alarming high symmetry, tetragonal $P4_2$ (*mnm*), with the 2^+ unit at a special site requiring D_{2h} symmetry. When it is considered that $1^+PF_6^-$ was disordered even with respect to the $(CH_2)_3$ and $(CH_2)_2$ bridges, it would certainly not be surprising if the $2^+PF_6^-$ crystals previously studied were actually bent at nitrogen, but disordered so that the sign of the bending angle was random, despite the respectable values of $R_1 = 0.063$ and $R_2 = 0.082$ observed. If 2^+ had been disordered and had a β(NN) of 15°, a real NN distance of 1.31 Å would give the apparent D_{2h} symmetry, β(NN) of 0°, and the observed NN bond length of 1.27 Å. We have no doubt that the $2^+PF_6^-$ structure we reported[4a] had undetected disorder and believe that the $1^+NO_3^-$ structure reported here reflects the geometry of a tetraalkylhydrazine radical cation far more accurately. Our incorrect belief that 2^+ was planar at nitrogen and has a shorter NN bond length than it does has colored our thinking for years,[2] and correcting those misimpressions is a significant result of this work.

The change in geometry upon electron removal from 1 to give 1^+ is still substantial. The NN bond length shortens 0.14_6 Å (9.9%). The nitrogens flatten substantially as well. The average of the bond angles at nitrogen, α_{av}, is 107.9° for neutral 1 and 115.6° for 1^+, so α_{av} changed from 1.6° less than the tetrahedral value of 109.5° to 6.1° greater than this value, which corresponds to 73% of the way from pure sp^3 hybridization to pure p hybridization ($\alpha_{av} = 120°$). Changes in geometry of the bicyclic system between 1 and 1^+ except for flattening at the nitrogens are rather small, the principal one being an increase in the C(1)N(8)C(5) angle from 101.3° to 105.5°.

3. Conformations of Neutral 1 in Solution. The ^{13}C NMR of 1 shows only four different carbons at +30 °C, but at −74 °C, the conformational interconversions are frozen on the NMR time scale and three conformations are detected. Due to the large steric requirements of the bis-bicyclic structure, only the four conformations shown below with a lone pair, lone pair dihedral angle of 180° are detectably occupied; the four conformations which would be reached by NN rotation to $\theta = 0°$ from the occupied

(6) Schenk, H.; MacGillavry, C. H; Skolnik, S.; Laan, J. *Acta Crystallogr.* **1967**, *23*, 423.

(7) Allinger, N. L. *J. Am. Chem. Soc.* **1977**, *99*, 8127. Program No. 395, Quantum Chemistry Program Exchange, Indiana University, Bloomington, IN.

(8) Dewar, M. J. S.; Thiel, W. *J. Am. Chem. Soc.* **1977**, *99*, 4889, 4907. Program No. 353, Quantum Chemistry Program Exchange, Indiana University, Bloomington, IN.

Table I. ^{13}C NMR Spectrum of **1** (50.4 MHz, CD_2Cl_2)

assign	δ (+30 °C)	δ (−74 °C)
C(1,5)	58.0 (d)[a]	59.8 (medium)[b] EA/AE[c]
		59.4 (large) EE
		55.1 (small) AA
		54.8 (medium) EA/AE
C(2,4)	30.0 (t)	33.0 (large) EE
		32.7 (medium) EA/AE
		23.6 (small) AA
		23.5 (medium) EA/AE
C(6,7)	27.1 (t)	27.6 (small) AA
		27.3 (large) EE
		26.9 (large) EA/AE
C(3)	17.1 (t)	17.3 (sh 17.1) all

[a] Multiplicity in off-resonance decoupled spectrum. [b] Relative peak size. [c] Assignment.

conformations are tremendously strained. Since the $(CH_2)_3$ bridges can be syn (s) or anti (a) to each other, and the NN bond can be axial (A) or equatorial (E) to a piperidine ring, four possible conformations exist, two of which, sEA and sAE, are indistinguishable, differing only in the numbering of the atoms. We

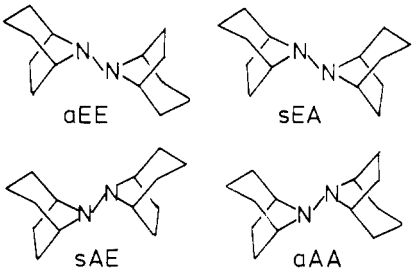

retain separate names for them only to simplify the discussion of energy differences. The ^{13}C NMR at −74 °C reveals that all these conformations are significantly populated. Because of the huge strain of 0° conformations, nitrogen inversion must accompany NN bond rotation in the conformational interconversion process. Due to the similar barriers between the conformations, the corresponding lines of all broaden at the same time, and we can only report an average $\Delta G^{\ddagger}$ for the NN rotation/N inversion process on the order of 12.3 kcal/mol.

The three types of CH_2 carbons in the ^{13}C NMR of **1** are easily assigned (Table I), for the $C_{2,4}$ carbon shows the largest γ effect and broadens the most, while C_3 is clearly the less intense and broadens the least as the temperature is lowered. Study of other 8-substituted-8-azabicyclo[3.2.1]octanes such as the N-methyl compound **4**[9] shows that C(2,4) and C(1,5) carbons in the E conformation will come significantly downfield from those in the A conformation, allowing confident assignment of the peaks in the frozen spectrum (Table I). Integration in the C(1,5) region gives relative areas of EA/AE 20, EE 37, AA 11, and EA/AE 18 units at −74 °C. These integrations give [aAA]/[aEE] = 11/37, corresponding to $\Delta G°$ (−74 °C) of aAA being 0.4_8 kcal/mol greater than that of aEE, and [SEA/[sAE]/[aEE] = ($^1/_2$)38/37, corresponding to $\Delta G°$ (−74 °C) of sEA/sAE being 0.2_6 kcal/mol higher than that of aEE. Within experimental error, then, it costs about 0.2_5 kcal/mol for each E bicyclooctane unit flipped to A.

We were initially surprised at the small energy difference between A and E bicyclooctane units in **1**, compared to the much larger differences in piperidines. We became even more confused when we could detect no A conformation for the chloroamine **5**, but comparison of chemical shifts of **5** with those for its bicyclononyl analogue **6**[10] make it clear that only E was observed.

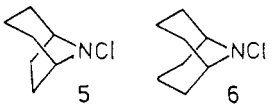

Table II. Comparison of Axial, Equatorial Substituent Energy Differences in Cyclohexanes, Bicyclo[3.2.1]octanes, and Their Nitrogen Analogues

compound	MM2 steric E diff ax-eq, kcal/mol	NMR $\Delta G°$(ax-eq), kcal/mol
7 	1.8	1.7[a]
8 	1.1	
9 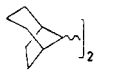	0.3[b]	
10 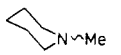	2.5	2.7[a]
4 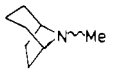	0.8	0.9[c]
1 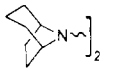		0.2_5[b,d]
11 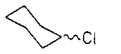	0.4	0.5[a]
12 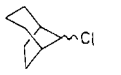	1.3	
13 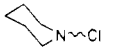		1.5[a]
5 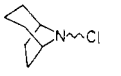		>ca. 1.2[d]

[a] Reference 11. [b] sEA vs. aEE. aAA vs. aEE is 1.0. [c] Reference 9. [d] This work.

In Table II we compare Allinger MM2 molecular mechanics calculations[7] with NMR results for several compounds. It may be seen that where comparison can be made (no force field is yet available for hydrazines or *N*-chloroamines), there is excellent agreement between calculated MM2 steric energy differences and NMR results. Most of the rather large steric destabilization of axial *N*-methylpiperidine disappears in the *N*-methylbicyclooctyl compound, but E is still considerably stabler than A in the *N*-chlorobicyclic compound **12**. The familiar 1,3 axial CH, axial NX interaction which destabilizes A forms of six-membered ring compounds is opposed in 8-substituted bicyclo[3.2.1]octane derivatives by the 1,2 interaction H(1)C(1), N(8)X(8), which is larger in E conformations than in A conformations because the H(1)C(1) and H(5)C(5) bonds are about 11–15° out of the C(1)N(8)C(5) plane (the range seen for MM2 geometries of various bicyclo[3.2.1]octane derivatives) and directed toward the $(CH_2)_2$ bridge, C(6)C(7), as indicated in the Newman projection down the N(8)C(5) bond shown as **14**. An axial C(8)/N(8)

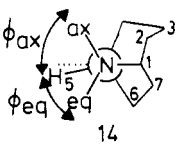

14

substituent has a larger (and hence more favorable) dihedral angle ϕ with H(1) and H(5) than does an equatorial substituent. The importance of this 1,2 interaction increases with the size of the

(9) Schneider, H.-J.; Sturm, L. *Angew. Chem., Int. Ed. Engl.* **1976**, *15*, 545.

(10) Nelsen, S. F.; Cunkle, G. T.; Gannett, P. M.; Ippoliti, J. T.; Qualy, R. J. *J. Am. Chem. Soc.* **1983**, *105*, 3119.

Table III. ESR and ENDOR Splitting Constant Data (in G)[e] for Some Bicyclic Hydrazine Radical Cations and Nitroxide

compound	1^+	2^+	15^+	16
method	ENDOR, ESR[a]	ENDOR, ESR[b]	ESR[a]	NMR, ESR[c]
a(N)[number]	13.7_3 [2]	13.3 [2]	13.6 [2]	20.25 [1]
$a(H_\beta)$	4.4_9 [4]	0.99 [4]	4.14 [4]	5.75 [2]
$a(H_{\gamma e}),C_{2,4}$	1.03 [4]	1.28 [8]	1.38 [4]	2.5 [2]
$a(H_{\gamma a}),C_{2,4}$	0.24 [4][d]	0.59 [8]	1.38 [4]	1.25 [2]
$a(H_{\gamma ex}),C_{6,7}$	*d*		unobsd	0.2 [2][d]
$a(H_{\gamma en}),C_{6,7}$	*d*		unobsd	0.1 [2][d]
$a(H_{\delta e}),C_3$	3.43 [2]	1.60 [4]		
$a(H_{\delta a}),C_3$	*d*	0.27 [4]		

[a] This work (1^+, CH_2Cl_2, 240 K; 15^+, *n*-PrCN, 233 K). [b] Reference 12. [c] Reference 13. [d] Not assigned completely to position. [e] 1 G = 0.1 mT ≃ 2.803 MHz.

substituent. For the 8,8′-bibicylco[3.2.1]octane **9** (see Table V), ϕ_{ax} is calculated by MM2 to be near 66° for A conformations and ϕ_{eq} to be near 45° for E conformations. We suggest this less favorable ϕ for the E conformation and the large steric demand of the C(8) substituent (a bicyclo[3.2.1]octane ring) is responsible for the much smaller A,E energy gap in **9** than in **8**, where the C(8) substituent is a methyl group. The relative importance of 1,3 and 1,2 interactions will also depend on the amount of bending at the atom at position 8 and the bond lengths to the bridgehead atoms. We presume greater bending at N than at C and smaller CN than CC bond lengths are responsible for A *N*-chloropiperidine (**13**) being so much less stable relative to the E form than is chlorocyclohexane (**11**). When this effect is coupled with the MM2 prediction of greater A destabilization for 8-chlorobicyclo[3.2.1]octane (**12**) than for **11**, it is clear that the data of Table V definitely predict that A **5** will be rather high in energy, and it is not surprising that we were unable to detect the A form.

It will be noted that **1** crystallizes as **1aAA**, the least stable of the detectable solution conformations. A plausible reason for this is that **1aAA** is the most compact conformation and is therefore expected to have higher attractive forces in the crystal. The MM2 calculations on the hydrocarbon analogues **9** demonstrate that this is the case. They give relative moments of inertia about the principal axes of 84, 218, and 225 for **9aAA**, 76, 244, and 244 for **9aEE**, and 81, 227, and 232 for **9aEA**, showing that the **aAA** form is indeed the most compact conformation.

4. Conformation of 1^+ in Solution. The proton hyperfine splitting for 1^+ (as for 2^+ [12]) proved to be so complex that we were unable to measure individual splittings from its ESR spectrum. ENDOR spectroscopy (in CH_2Cl_2 at −33 °C) allowed measurement of four different proton splittings as well as a(2N); see Table III. Simulations of the ESR spectrum using these splittings showed that the 4.49- and 1.03-G splittings correspond to 4H each, but that the 3.43-G splitting corresponds to only two hydrogens. This two-hydrogen splitting can only be attributed to the $H_{\delta e}$ hydrogen at C(3) of each ring, by analogy with the assignments of the $H_{\delta e}$ and $H_{\delta a}$ splittings in 2^+.[12] The ESR spectrum of the 3,3′-keto analogue of **1**, **15**, is surprisingly simple and shows a 4.14-G 4H splitting and a 1.38-G splitting for 8H. Exchange

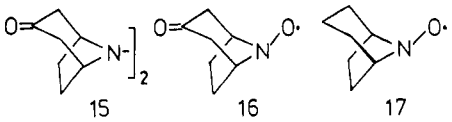

15 16 17

of all the protons at C(2) and C(4) for deuterium showed that the $H_{\gamma e}$ and $H_{\gamma a}$ hydrogens at C(2) and C(4) are responsible for the eight hydrogens showing splittings of 1.3, G and require assignment of the bridgehead hydrogens as the 4.14-G splitting, thus allowing the assignments shown in Table III for 1^+. Splittings from the hydrogens at C(6,7) were not observed for **1** or **15**, which is not surprising considering their small size in nitroxide **16**, where they were measured by the more sensitive NMR technique.[13]

Rassat and Rouzaud have discussed the γ- and δ-hydrogen splittings for nitroxides **16** and **17** in detail and pointed out that they are only compatible with the bend at N(8) being in the *axial* direction.[13] **16** and its bridgehead dimethyl analogue have also been shown to be bent axial in their crystals.[14] Axial bend at N(8) is also required for 1^+. The 3.43-G H_δ splitting can only be assigned to $H_{\delta e}$, and it is about twice as large as for $H_{\delta e}$ of 2^+. Axial bend at N lines up the spin-bearing orbital for most favorable spin transmission to $H_{\delta e}$, and the alignment is far less favorable for equatorial bend. The two directions of bend are isoenergetic in the bicyclononyl system, so each $H_{\delta e}$ is averaged between a high and a low splitting value. From the discussion of A vs. E energies in the neutral compounds, it is now clear why both the nitroxides and the hydrazines in the bicyclo[3.2.1]octyl system favor axial bend. Their nitrogens are much flatter than those of diamagnetic compounds, cutting down the 1,3 interaction in the A conformation and increasing the size of the 1,2 interaction with the bridgehead hydrogens in the E conformation.

Because the nitrogens are equivalent in 1^+ and 2^+, the spin densities at N are equal in these systems, so the bridgehead splittings provide a simple estimate of the amount of bend at nitrogen, which was not available to Rassat and Rouzaud for the nitroxides because of uncertainty in ρ(N). The simple form of the β splitting McConnel equation $a(H_\beta) = A_\beta \rho_N^\pi \langle \cos^2 \theta \rangle$ is only designed to work when the spin-bearing orbital is nearly pure p in its hybridization. Hydrazine radical cations, which are easy to bend at nitrogen, show unusually large a(N) differences as the alkyl groups are changed, reflecting different average amounts of bend. Nevertheless, despite the fact that a(2N) varies from 13 to 19 G for various $(RMeNNMeR)^+$ examples, and a(N) increases as bending increases, $a(CH_3)$ remains constant at 12.7 ± 0.3 G.[15] Because $\langle \cos^2 \theta \rangle = 0.5$ for a methyl group, this demonstrates that $Q_\beta \rho_N^\pi$ is effectively constant at 25.4 G for tetraalkylhydrazines which differ considerably more in their amount of bend at nitrogen than do 1^+ and 2^+. Only an averaged $\langle \cos^2 \theta \rangle$ is being observed by the ESR experiment, because the a(H) observed is time-averaged over a range of bending values for compounds as easily bent as hydrazine radical cations. Nevertheless, the bridgehead proton splittings for 1^+ and 2^+ show that their average β(NN) values are very close in solution. Since θ is the H(1)C(1), N1 p dihedral angle, to estimate β(NN) from a(H(1)), it is necessary to know how β (lone pair) is related to β(NN). (See **18**). We calculated the relationship by using

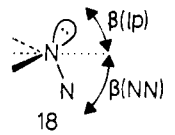

18

natural hybrid orbital INDO calculations on NH_3, employing the program BONDO, written by Weinhold.[16] It is, of course, not strictly correct to estimate an average $\langle \theta \rangle$ from an average $\langle \cos^2 \theta \rangle$, but this is the best that we can do.

Estimation of the angle $\langle \theta \rangle$ in the bicyclononyl and bicyclooctyl systems (we used the MNDO calculated H(1), C(1), N(8), C(5) geometry) gave the following results. The 0.99-G bridgehead splitting of 2^+ corresponds to $\langle \theta \rangle$ of 78.6°, which gives β(NN) of about 18°. The 4.49-G bridgehead splitting of 1^+ corresponds to $\langle \theta \rangle$ of 65.1°, also corresponding to β(NN) of about 18°. We believe that the bridgehead proton ESR splitting shows that 1^+

(11) Anet, F. A. L.; Yavari, I. *Tetrahedron Lett.* **1977**, 3207 and references therein.

(12) Gerson, F.; Lopez, J.; Nelsen, S. F.; Akaba, R. *J. Am. Chem. Soc.* **1981**, *103*, 6716.

(13) (a) Rassat, A.; Rouzaud, J. *Tetrahedron* **1976**, *32*, 239. (b) Rassat, A.; Rouzaud, J. *J. Am. Chem. Soc.* **1971**, *93*, 5041.

(14) (a) Capiomont, A.; Chion, B.; Lajerowciz, J. *Acta Crystallogr., Sect. B* **1971**, *27B*, 322. (b) Capiomont, A. *Acta Crystallogr., Sect. B* **1973**, *B29*, 1720.

(15) Nelsen, S. F.; Weisman, G. R.; Hintz, P. J.; Fahey, M. R. *J. Am. Chem. Soc.* **1974**, *96*, 2916.

(16) BONDO is described in detail in: Weinhold, F. A., University of Wisconsin Theoretical Chemistry Institute Technical Note 628G, Dec 1979.

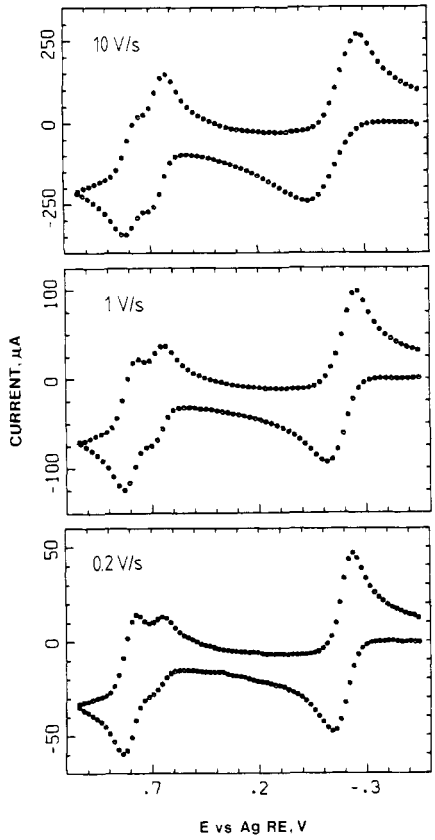

Figure 5. Cyclic voltammograms of **1** at 22 °C, 3.6 × 10^{-3} M, as a function of scan rate.

cannot be as bent at nitrogen in solution as it is in the crystal, where β(NN) is 32.5°, because this β(NN) value would lead to an a(H(1)) value of 7.1 G, which is unreasonably larger than what is observed. The MNDO structure of $\mathbf{1}^+$ in the aAA geometry predicts a β(NN) value of 17.3° (see below). We are not surprised that crystal packing forces impose a larger β(NN) value in the crystal than in solution. Increasing β(NN) makes $\mathbf{1}^+$ more compact, and we have already seen that in the neutral form they cause **1** to crystallize out in the aAA conformation, which is the least stable solution conformation. The bridgehead proton splitting of $\mathbf{2}^+$ indicates that the nitrogen is significantly pyramidal in solution, which is consistent with it also being pyramidal in the solid.

5. Cyclic Voltammery of 1. The CV experiment on **1** at room temperature in acetonitrile containing 0.1 M tetra-*n*-butylammonium perchlorate (the conditions used for most of our work comparing thermodynamics of electron loss for hydrazines[2]) exhibits a chemically reversible first oxidation wave at $E°_1'$ +0.13 V vs. SCE but two chemically reversible second oxidation waves at $E°_2'$ +1.01 and 1.14 V. The relative size of the $E°_2'$ waves is scan rate dependent. The ratio of the species giving the 1.01-V wave to that giving the 1.14-V wave is about 1.45 at scan rates above 5 V/s, but the 1.14-V wave increases in relative size at slower scan rates (see Figure 5). Solid $\mathbf{1}^+NO_3^-$ exists exclusively in the anti form, $\mathbf{a1}^+$, and dissolution of either the nitrate or the hexafluorophosphate at low temperature gives only the 1.14-V wave, proving that this wave corresponds to oxidation of $\mathbf{a1}^+$ to $\mathbf{a1}^{2+}$. A supporting electrolyte concentration of 0.14 M was used in all the quantitative equilibrium and rate constant studies because it improved the wave shape of the low-temperature CV curves. At higher temperatures, a small contribution of the 1.01-V wave is detectable when $\mathbf{1}^+$ solutions are oxidized (see Figure 6). We attribute the $E°'$ = 1.01 wave to the $\mathbf{s1}^+$, $\mathbf{s1}^{2+}$ electron transfer (see Scheme I). The ratio of the concentrations of $\mathbf{s1}^+$ to $\mathbf{a1}^+$ was determined by simulation of the CV of equilibrated $\mathbf{1}^+$ solutions, giving 0.07 ± 0.01_0 at 6 °C, 0.08_4 ± 0.01_5 at 22 °C, and 0.11 ± .01 at 48 °C. The onset of dication decomposition was already noted in the CV experiments at 48 °C, precluding extending the temperature range reliably. The data at 22 °C correspond to $\Delta G°(\mathbf{a1}^+,\mathbf{s1}^+)$ = 1.45 ± .12 kcal/mol (see eq 2),

$$\mathbf{a1}^+ \underset{k_1}{\overset{k_{-1}}{\rightleftharpoons}} \mathbf{s1}^+ \quad \Delta G°(22\ °C) = 1.4_5\ \text{kcal/mol} \qquad (2)$$

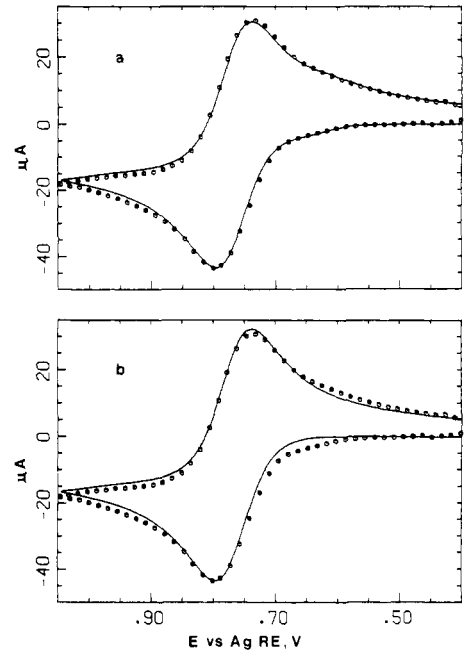

Figure 6. Cyclic voltammogram of $\mathbf{1}^+$ at 2.5 × 10^{-3} M, 17 °C, 0.5 V/s scan rate (circles) compared with simulations (lines) using (a) 9% of a minor isomer, (b) no minor isomer.

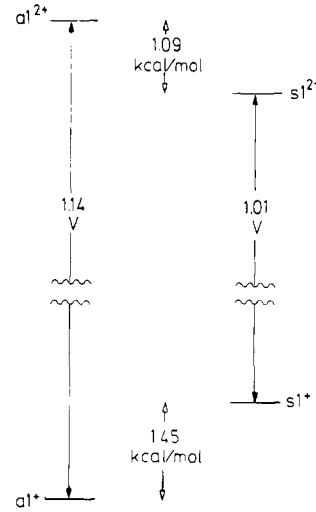

Figure 7. Energy diagram for **s**- and $\mathbf{a1}^+$ and $\mathbf{1}^{2+}$

Scheme I

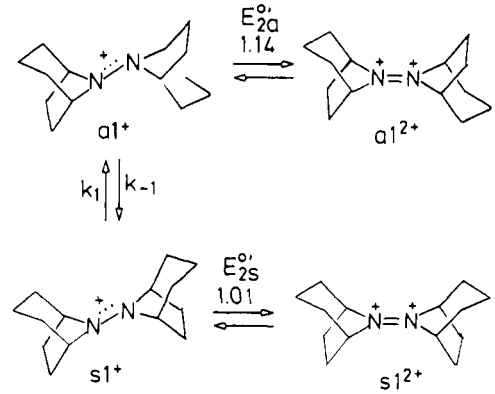

Table IV. Kinetic Results for NN Bond Rotation in 1^+

temp, °C	method	k_{obsd},[a] 10^4 s^{-1}	K_{eq} (s/a)	k_1(s → a), 10^4 s^{-1}	$\Delta G^{\ddagger}$(s → a), kcal/mol
6.0	CV	0.60_2	0.070	0.56_3	21.7
11.6	CV	1.04	0.075	0.96_7	21.9
16.6	CV	1.71	0.080	1.58	22.0
17.2	CV	1.94	0.080	1.80	22.0
17.3	UV	1.75	0.080	1.62	22.0
17.8	CV	1.98	0.080	1.83	22.0
23.8	UV	3.81	0.085	3.51	22.1
28.3	UV	8.41	0.090	7.72	21.9
28.7	UV	8.02	0.090	7.36	22.0
34.7	UV	18.7	0.095	17.1	21.9
40.9	UV	32.5	0.105	29.4	22.1

and the temperature dependence observed corresponds to ΔH° = 1.92 kcal/mol, ΔS° = +1.6 cal/(mol deg) (Figure 7). The ΔS° observed is close to the 1.4 kcal/mol expected by symmetry assuming $\mathbf{a1}^+$ exists exclusively in the AA form (NN bond axial to each piperidine ring) observed in the solid and inferred from ENDOR measurements in solution, while $\mathbf{s1}^+$ is a 1:1 mixture of AE and EA forms. Not trusting the 48 °C data as much because of the slight decomposition observed, we employed ΔH° = 1.8_6 kcal/mol and ΔS° = 1.4 cal/(mol deg) in the calculations of the equilibrium concentrations used in the kinetic analysis below.

These data allow construction of the free-energy diagram shown in Figure 3. There is a reversal in stability of *syn*- and *anti*-**1** between the radical cation and dication. The turnaround in stability of s and a forms in the dications is crucial in allowing the CV analysis, because $\Delta E^\circ{}_2{}'$ would only be 0.06_3 V if the dications had the same energy, which would make measurement of the isomer ratio both difficult and not very accurate.

6. Rotational Barrier of 1^+ by CV. All that is needed to allow measurement of the rotational barrier for 1^+, then, is generation of a nonequilibrium mixture of the s and a forms, so that the rate of approach to equilibrium in eq 2 can be monitored by cyclic voltammetry. The CV of **1** at room temperature demonstrates that the rapid oxidation of the equilibrium mixture of neutral forms generates about a 1.45:1 ratio of $\mathbf{s1}^+/\mathbf{a1}^+$, but the rapid increase in the fraction of the $\mathbf{a1}^+$ isomer as the scan rate is lowered indicates that there will be a problem in generating a nonequilibrium mixture by rapid oxidation. Neutral **1** catalyzes the isomerization of $\mathbf{s1}^+$ to $\mathbf{a1}^+$ (which is discussed in detail in section 9), and we were unable to generate 1^+ solutions which differed significantly from the equilibrium mixture by either chemical or electrochemical oxidation. The small equilibrium concentration of $\mathbf{s1}^+$ precludes obtaining accurate kinetics on its formation from the solutions of pure $\mathbf{a1}^+$ available by solution of crystalline 1^+ salts. Photolysis provides a way of "pumping" 1^+ solutions to a nonequilibrium mixture of s and a isomers. Irradiation populates the π, π^* excited state, which has two antibonding and only one bonding π electrons and therefore an overwhelming electronic preference for perpendicular π atomic orbitals at the nitrogens, and demotion leads to both $\mathbf{s1}^+$ and $\mathbf{a1}^+$. Low-intensity photolysis (Sylvania 275-W sunlamp, through Pyrex glassware) proved to yield a photostationary state with a ratio of $\mathbf{s1}^+/\mathbf{a1}^+$ of about 1.6, but even under these conditions, extended photolysis leads to decomposition of 1^+. For the kinetic work, we used about 90 s of photolysis, which generates an s/a ratio of over 1 without any detectable decrease in the total current for 1^+, 1^{2+} oxidation and followed the return to equilibrium in the dark, by cyclic voltammetry. The relative amounts of $\mathbf{s1}^+$ and $\mathbf{a1}^+$ were determined by simulation of the CV curves. The reaction was followed for about 2.5 half-lives; changes in the relative amounts of $\mathbf{s1}^+$ and $\mathbf{a1}^+$ become too small for accurate ratio determination at later times. The CV before irradiation was used as the infinity point. Because it is necessary to stir between obtaining points, but the solution must be still to have the true diffusion currents calculated for the simulation of the isomer ratios, we could not use the CV method when the half-life for equilibration was under about 1 h, limiting the upper temperature usable to about 18 °C. Data workup is extremely time-consuming because of all the CV simulations required. The results of the CV measuremnts of 1^+ isomerization are shown in Table IV.

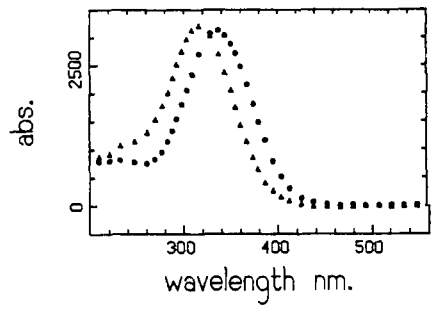

Figure 8. UV spectra for $\mathbf{s1}^+$ and $\mathbf{a1}^+$. Circles, anti; triangles, syn. The vertical axis represents ϵ values.

7. UV Spectra of 1^+. Because the isomerization is a first-order process, we can follow it to obtain rate constants with any parameter which varies linearly with concentrations of the isomers. We were initially surprised that photolysis led to a 1.6 ratio of $\mathbf{s1}^+$ to $\mathbf{a1}^+$, because demotion of the perpendicular π, π^* excited state of 1^+ ought to give equal amounts of the two isomers, as it is known to do for olefins such as 2-butene.[17] Seeing an isomer ratio different from 1 implied that the UV absorption spectra of $\mathbf{s1}^+$ and $\mathbf{a1}^+$ were significantly different. Obtaining a UV spectrum before and after irradiation and measuring the isomer ratio by CV for both solutions allow deconvolution into the UV spectra of the two isomers by solving simultaneous linear equations for each point of the digitized spectra. The result of this deconvolution is displayed as a comparison of UV spectra for $\mathbf{s1}^+$ and $\mathbf{a1}^+$ in Figure 8. The high-wavelength region of Figure 8 is certainly more accurate than the low-wavelength region, because extended photolysis generates low-wavelength absorptions as the absorption maximum near 330 nm decreases. The shapes of the UV curves for the isomers are nearly the same, but $\mathbf{a1}^+$ has λ_m of 337 nm and $\mathbf{s1}^+$ 318 nm. We were surprised at the blue shift of 19 nm for $\mathbf{s1}^+$, but subsequent work on other hydrazine radical cations has made this understandable.[4] The π, π^* absorption maximum for hydrazines moves to longer wavelengths as bending at N increases because of unusually large σ, π mixing effects. $\mathbf{s1}^+$ is less bent at nitrogen than is $\mathbf{a1}^+$, because it must have an equatorial R_2N substituent, and 1,2 interaction with the bridgehead hydrogens is more serious with equatorial R_2N substituents than with axial ones. From the size of the bridgehead hydrogen splitting in the ENDOR spectrum of $\mathbf{a1}^+$,[2b] this species cannot be as bent in solution as it is in the solid, where β(NN) is 32.5°; we estimated in section 4 a value of 18° from the size of the bridgehead hydrogen splitting. In keeping with this expectation of greater bending and hence longer wavelength maximum in the solid than in solution, a Nujol mull of $1^+NO_3^-$ showed a λ_m of 346–348 nm (the absorption band is broader in the solid than in solution). The question of a medium effect causing the 10-nm red shift in $\mathbf{a1}^+$ in the solid compared to solution was investigated by examining the spectra for $\mathbf{2}^+PF_6^-$ in acetonitrile (λ_m 340 nm[19]) and in a Nujol mull (λ_m 335–337 nm). As discussed in section 4, we believe crystalline and solution 2^+ have similar amounts of bend at nitrogen, in contrast to 1^+. We therefore argue that the UV spectrum of $\mathbf{a1}^+$ provides additional evidence for a significant difference in its amount of bend at nitrogen in the solid and in solution.

(17) For a review see: Saltiel, J.; D'Agostino, J.; Megarity, E. D.; Metts, L.; Neuberger, K. R.; Wrighton, M.; Zafarious, O. C. *Org. Photochem.* **1973**, *3*, 1–113.

(18) Nelsen, S. F.; Blackstock, S. C.; Yumibe, N. P.; Frigo, T. B.; Carptenter, J. E.; Weinhold, F. *J. Am. Chem. Soc.* **1985**, *107*, 143.

(19) Nelsen, S. F.; Teasley, M. F.; Kapp, D. L.; Kessel, C. R.; Grezzo, L. A. *J. Am. Chem. Soc.* **1984**, *106*, 791.

Scheme II

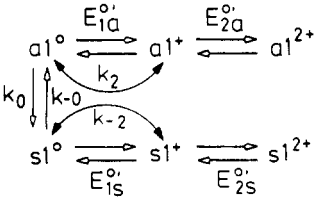

8. Rotational Barrier for 1^+ by UV. For the UV measurement of the rotational barrier, a sample of 1^+ in a thermostated UV cell holder was irradiated at 366 nm until the absorption at 360 nm had dropped about 0.1 unit, and the absorbance was followed at 360 nm for about 10 half-lives to allow measurement of an accurate end point. The rate constants thus determined are compared with those from CV in Table IV and in the Eyring plot of Figure 9. The UV experiments were done at about one-quarter the concentration of the CV experiments (0.6–0.7 mM vs. 2.5–2.7 mM), further establishing the first-order kinetics of the isomerization. We were gratified to obtain such good agreement between two quite different methods for measuring k_1 and to be able to extend the temperature range for our experiments to 35 °C because data may be taken so much faster by UV than by CV. These data give for $k_1(\mathbf{s1}^+ \rightarrow \mathbf{a1}^+)$ $\Delta H^{\ddagger} = 20.2 \pm 1.6$ kcal/mol, $\Delta S^{\ddagger} = -5.9 \pm 5.5$ cal/(deg mol), at 25 °C $\Delta G^{\ddagger} = 21.9_8 \pm .06$ kcal/mol, and $\Delta G^{\ddagger}$ ($\mathbf{a1}^+ \rightarrow \mathbf{s1}^+$) 23.4 kcal/mol, because $\mathbf{a1}^+$ is 1.4_7 kcal/mol more stable than is $\mathbf{s1}^+$.

9. Homogeneous Electron Transfer between 1 and 1^+ by CV. The interconversion of $\mathbf{a1}^+$ and $\mathbf{s1}^+$ detected by CV at slower scan rates in Figure 5 is far too fast to be accounted for by NN bond rotation in the radical cations and undoubtedly involves electron transfer between neutral **1** and its cation radical, as indicated in eq 3. Although eq 3 clearly affects the CV at slow scan rates,

$$\mathbf{s1}^0 + \mathbf{a1}^+ \underset{k_{-2}}{\overset{k_2}{\rightleftharpoons}} \mathbf{s1}^+ + \mathbf{a1}^0 \qquad (3)$$

it does not isomerize $\mathbf{s1}^+$ to $\mathbf{a1}^+$ detectably at scan rates above 5 V/s, so it must actually be relatively slow.

The CV curves for **1** oxidation therefore contain information on k_2 and k_{-2}, although it is difficult to extract because of the complexity of the system. The rapid interconversion and similar energies of **a1EE** and **a1AA** led us to make the simulation more manageable by grouping them as $\mathbf{1a}^0$. The $\mathbf{s1}^0 \rightleftarrows \mathbf{a1}^0$ interconversion is rapid at ambient temperature, and we showed that curves calculated allowing them to interconvert with a barrier of 12.3 kcal/mol (see section 3) were identical with those generated by treating them as instantaneously at equilibrium, so the rest of the simulations were done with the latter assumption, which saves computer time. Scheme II was used for the initial simulations. Because the cation radical and the NN bond rotational rates k_1 and k_{-1} are too slow to be of consequence in the CV experiments, the only two nonelectrochemical parameters in Scheme II are the $\mathbf{s1}^0/\mathbf{a1}^0$ equilibrium constant and the homogeneous electron transfer rate k_2. These parameters were varied until the best fit was obtained at all scan rates, giving a $\text{syn}^0/\text{anti}^0$ ratio of 1.45 and a k_2 value of 2.6×10^2 s^{-1} M^{-1} ($k_{-2} = 5.4 \times 10^6$ s^{-1} M^{-1}). Slow heterogeneous electron-transfer kinetics affected the data at the fast scan rates so the values of the heterogeneous electron-transfer rate constants were varied to produce simulations in which the peak separations agreed with experiment. Close inspection of the simulation reveals that although the fast scan rate data fit rather well, slightly too little $\mathbf{a1}^{2+}$ and too much $\mathbf{s1}^{2+}$ reduction current was observed at slow scan rates relative to the calculated values (Figure 10a, supplementary material). This poor fit only affects the dication reduction peaks, not their oxidation peaks, so it cannot be fixed by varying either of the two adjustable parameters in Scheme II. We concluded that the model was oversimplified and that the dications were involved in nonelectrode reactions. There is certainly no shortage of these available, and several are written down as eq 4–8.

$$\mathbf{a1}^{2+} + \mathbf{s1}^+ \rightleftarrows \mathbf{a1}^+ + \mathbf{s1}^{2+} \qquad (4)$$

$$\mathbf{s1}^{2+} + \mathbf{s1}^0 \rightleftarrows 2\mathbf{s1}^+ \qquad (5)$$

$$\mathbf{s1}^{2+} + \mathbf{a1}^0 \rightleftarrows \mathbf{s1}^+ + \mathbf{a1}^+ \qquad (6)$$

$$\mathbf{a1}^{2+} + \mathbf{a1}^0 \rightleftarrows 2\mathbf{a1}^+ \qquad (7)$$

$$\mathbf{a1}^{2+} + \mathbf{s1}^0 \rightleftarrows \mathbf{a1}^+ + \mathbf{s1}^+ \qquad (8)$$

The dication, radical cation electron transfer of eq 4 provides a way to interconvert $\mathbf{s1}^{2+}$ and $\mathbf{a1}^{2+}$, and its equilibrium constant may be calculated from the known $E^{0\prime}$ values to be 140; the stabler radical cation and dication are both on the right. Addition of eq 4 as a process so rapid that it is always at equilibrium causes the fit of the calculated dication reductive waves to the experimental data to actually become worse. The dication, neutral disproportionation reactions (eq 5–8) are all more than 18 kcal/mol exothermic and are therefore expected to be rapid and proceed essentially to completion. Addition of these reactions to Scheme II significantly improved the fit of the dication reduction waves at slow scan rates (Figure 10b, supplementary material). The disproportionation reactions were treated as diffusion-limited irreversible reactions and are necessary to achieve good simulations at all scan rates. Interestingly, inclusion of eq 4 along with eq 5–8 in the reaction scheme had no observable effect on the calculations, so we are unable to speculate on its occurrence. The greatly expanded scheme including eq 4–8 improved the fit of the dication reduction waves noticeably, but did not change the best fit parameters of Scheme II from $K_{eq} = 1.45$, $k_2 = 2.6 \times 10^2$ s^{-1} M^{-1}, at 3.6×10^{-3} M **1**, 22 °C (see supplementary material Figures 11 and 12 for these simulations). The electron-transfer reaction is bimolecular and should show concentration dependence, so samples at 5.6×10^{-3} and 0.5×10^{-3} M were also studied and fit with the same parameters. We observed reasonably good fit at all concentrations and an obviously faster isomerization rate at high **1** concentrations, which provides additional support for the bimolecular pathway proposed. The equilibrium constant for eq 3 can be calculated from the free-energy changes of reactions 9 and 2: $\Delta G^{\circ}_2(22\ ^{\circ}\text{C}) = 1.6_7$ kcal/mol, $K_2 = 5.8 \times 10^{-2}$. The

$$\mathbf{a1}^0 \underset{k_{-0}}{\overset{k_0}{\rightleftharpoons}} \mathbf{s1}^0 \quad \Delta G^0(22\ ^{\circ}\text{C}) = -0.2_2 \text{ kcal/mol} \qquad (9)$$

value of 260 s^{-1} M^{-1} for k_2 corresponds to $\Delta G^{\ddagger}_2$ of 14.0 kcal/mol, with an accuracy estimated from changing rates in the simulations of ±0.3 kcal/mol; $k_{-2} = 4.5 \times 10^3$ M^{-1} s^{-1}, $\Delta G^{\ddagger}_{-2} = 12.3 \pm 0.6$ kcal/mol.

Although the conformational interconversions of neutral **1** are rapid on the CV time scale at room temperature, fast scan rates at lower temperature do cause a shoulder to appear on the anodic side of the $\mathbf{1}^0$, $\mathbf{1}^+$, wave, which corresponds to the $\mathbf{s1}^0$, $\mathbf{s1}^+$ redox couple. This couple must show an $E^{0\prime}$ value positive of the $\mathbf{a1}^0$, $\mathbf{a1}^+$ couple because there is a larger energy gap between the neutral and cation in the syn than anti forms. The temperature and scan rate dependence of the first oxidation wave were simulated as a check on the syn/anti ratio obtained for the room-temperature CV (from the ratio of $\mathbf{s1}^+$, $\mathbf{s1}^{2+}$ oxidation waves at fast scan rates) and the nitrogen inversion/NN rotational barrier estimated by ^{13}C NMR (at 10^3 greater concentration, in a different solvent, at much lower temperature). We once again lumped **a1EE** and **a1AA** together because their CV curves were not resolved due to their small energy difference. The radical cation rotational barrier is too high to have any effect. Reasonable fit was obtained by using $K_{eq} = [\mathbf{s1}^0]/[\mathbf{a1}^0]$ of 1.3 and $\Delta G_0^{\ddagger}$ ($\mathbf{a1}^0 \rightarrow \mathbf{s1}^0$) of 12.5 ± 0.3 kcal/mol at −14.5°, and $K_{eq} = 1.1$, $\Delta G^{\ddagger}_0 = 12.0 \pm 0.3$ kcal/mol at −39.5°. A ΔE°_1 value of 0.1 V was needed to produce reasonable fits. The large overlap of the two waves due to small differences in oxidation potentials and broadening due to slow heterogeneous electron-transfer constants make comparison of the calculated and experimental curves rather imprecise, but the agreement with the room-temperature experiments on the second oxidation waves where K_{eq} of 1.45 at 22 °C gave best fit is reasonably good. There is a clear trend to smaller K_{eq} at lower temperature, which is qualitatively consistent with the NMR-derived K_{eq} value of less than 1 at −74 °C, although the effect

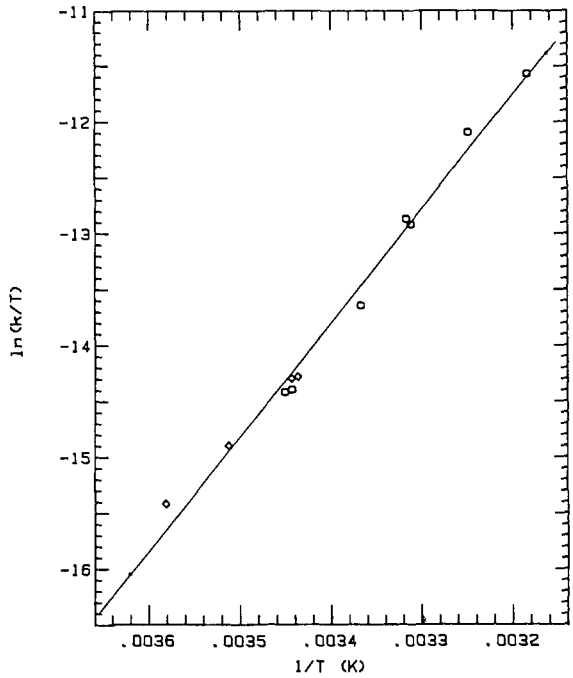

Figure 9. Eyring plot of the kinetic data of Table I. Circles measured by UV, diamonds, measured by CV.

of changing solvent may well not be negligible. The $\Delta G^{\ddagger}_0$ barriers determined above are also not far from the NMR coalescence value of 12.3 at about −20 °C. The $\Delta E^{\circ}_1{}'$ of 0.1 V needed for simulation is clearly too large and presumably has something to do with the unaccounted for **a1AA** conformer, which will oxidize more easily than the **a1EE** conformer. Only crude values are available from these simulations, but they do show that the values obtained by other experiments do not give results which conflict seriously with experiment for the first oxidation wave of **1**.

10. Homogeneous Electron Transfer between 1 and 1^+ by UV. Addition of a small amount of neutral **1** to the 1^+ sample should catalyze the isomerization of $\mathbf{s1}^+$ to $\mathbf{a1}^+$ through eq 3. Because isomerization of $\mathbf{a1}^0$ to $\mathbf{s1}^0$ is fast compared to the other reactions, they should remain at their equilibrium concentration throughout the reaction, and the 1^+ equilibrium should be approached with an observed first-order rate constant of $k_{obsd} = k_{-2}[\mathbf{a1}^0] + k_2[\mathbf{s1}^0] + k_1 + k_{-1}$. This statement was checked by using the digital simulation program RATES[20] which displays concentrations of each species as a function of time. Varying $\Delta G^{\ddagger}_0$ barriers from 12.3 to 15.0 kcal/mol gave perfect first-order kinetics. A UV sample of 6.0×10^{-4} M 1^+ and 1.2×10^{-3} M 1^0 in CH_3CN was photolyzed and the equilibrium monitored at 11.3 °C, giving k_{obsd} of 1.16×10^{-3} s^{-1}. Knowing that $k_1 + k_2$ is 1.04×10^4 s^{-1} at 11.3 °C and using a value of 1.45 for $K_{eq} = \mathbf{s1}^0/\mathbf{a1}^0$ gives $k_{-2} = 2.0 \times 10^3$ M^{-1} s^{-1} and $k_2 = 1.05 \times 10^2$ M^{-1} s^{-1}, so $\Delta G^{\ddagger}_{-2}$ is 12.3 and $\Delta G^{\ddagger}_2$ is 14.0 kcal/mol. The excellent agreement with the numbers derived by the very different method of CV simulation at 22 °C gives us added confidence that we actually know the barriers for homogeneous electron transfer of the 1^0, 1^+ isomers.

11. MNDO Calculations on 1^+ and 1^{2+}. The most interesting conformational question brought up in our electrochemical work which is not addressed by the studies on 1^+ is why *syn*-1^{2+} is about 1 kcal/mol more stable than is the anti form. The reason we initially guessed that the more stable rotamer of 1^+ might be syn (which we have shown above to be incorrect) was the fact that the more stable radical cation has the least stable dication, as determined from cyclic voltammetry work. We thought that syn ought to be the least stable dication due to a larger steric interaction between the bridgehead hydrogens. The olefins **19** ought to be good models for the dications, and although MM2 calculations give the result that **s19** is less stable than **a19**, the amount is only 0.08 kcal/mol. Redefining the sp^2–sp^2 bond length to 1.22 Å and the sp^2–sp^3 bond length to 1.40 Å to account for the shorter bonds in the tetraalkyldiazenium dication increases the energy difference, but only to 0.45 kcal/mol. Thus a steric argument predicts that *anti*-1^{2+} would be more stable than *syn*-1^{2+}, but only by a small amount. We therefore attempted MO calculations to see if the turnaround in **s** vs. **a** stability for 1^+ and 1^{2+} could be rationalized and also to see how close MO calculations would get the geometry of 1^+ to the experimentally determined geometry. For molecules the size of **1**, only semiempirical calculations are currently feasible, and complete geometry minimization (44 bondlengths, angles, and dihedral angles) MNDO calculations[8] were done on the symmetrical **aAA** and **sEE** conformations on both 1^+ and 1^{2+}, giving the results in Table V.

Table V. MNDO Energy Minimized Calculations

species	ΔH_f, kcal/mol	d(NN), Å	β(NN), deg
$\mathbf{1aAA}^+$	173.1	1.302	17.3
$\mathbf{1sEE}^+$	174.0	1.295	7.1
$\mathbf{1sAE}^{+a}$	174.0	1.299	18.7, 8.0
$\mathbf{1aAA}^{2+}$	466.4	1.238	0.5
$\mathbf{1sEE}^{2+}$	467.0	1.238	0.9

[a] Not completely minimized. See text.

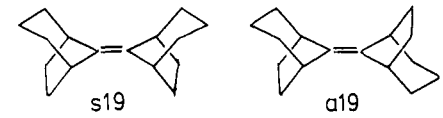

MNDO correctly gets *anti*-1^+ more stable than *syn*-1^+, and also correctly gets the aAA form as the stablest anti conformation for $\mathbf{1aAA}^+$. The β(NN) value for **1aAA** of 17.3° is actually closer to the approximately 18° estimated from the ENDOR bridgehead hydrogen splitting than is the X-ray structure of the crystalline solid. The MNDO NN bondlength is only about 0.02 Å shorter than the X-ray bond length, and flattening at N ought to decrease the NN bond length. We note that MNDO calculations are surprisingly successfuly for $\mathbf{1aAA}^+$ and certainly more successful than on neutral hydrazines. We presume this is because one of the lone pair electrons has been removed; MNDO does not treat the lone pair, lone pair interactions in hydrazines very well. We expect the stablest form of *syn*-1^+ to be the **sAE** form, but we were unable to calculate its energy properly, since it would have almost twice as many quantites to minimize (the two bicyclic rings are different in the **sAE** form). We did an approximate calculation of $\mathbf{1sAE}^+$ by rotating the minimized $\mathbf{1aAA}^+$ structure 180° about the NN bond (to **1sAA**) and bending one ring to the E position but minimizing only on d(NN), d(CN), and the two β(NN) values. The ΔH_f obtained was 0.02 kcal/mol below that of completely minimized $\mathbf{1sEE}^+$, so we do not doubt that complete minimization would decrease the ΔH_f of $\mathbf{1sAE}^+$ a little, but expect it not be much more stable than the partially minimized structure of Table VII. We note that the nitrogen of E-bent 1^+ is predicted to be significantly flatter than that of A-bent 1^+, presumably caused by the steric interaction of the R_2N group with the bridgehead hydrogens of the E-bent bicyclic ring.

MNDO predicts the anti dication to be more stable than the syn one, as expected on steric grounds, and the nitrogens are essentially flat in both structures. The dication $(N{=}N)^{2+}$ bond length is calculated to be 1.24 Å, within the experimental range of 1.22–1.25 Å observed for saturated azoalkanes.[3] The experimentally observed turnaround of stability of the anti and syn rotamers of 1^+ and 1^{2+} is not calculated by MNDO. We conclude that the turnaround in stability observed in solution which makes $\mathbf{1s}^{2+}$ more stable than $\mathbf{1a}^{2+}$ is unlikely to have a steric or electronic origin within the hydrazine dication unit. The experimental data are for solvated ions in solution. Anion approach ought to be easier for the syn form, in which the counterion ought to be able to approach more closely to the side blocked by two $(CH_2)_2$ bridges than in the anti form, where both sides have $(CH_2)_2$ and $(CH_2)_3$

(20) RATES uses a polyalgorithm for the numerical solution of ordinary differential equations. Byrne, O. D.; Hindmarsh, A. C., UCRL-75652, Lawrence Livermore Laboratory, Livermore CA.

Scheme III

step 1 $2a1^+ \rightleftharpoons a1^{2+} + a1^\circ$

step 2 $a1^\circ + s1^+ \underset{k_2}{\overset{k_{-2}}{\rightleftharpoons}} a1^+ + s1^\circ$

step 3 $a1^{2+} + s1^+ \rightleftharpoons a1^+ + s1^{2+}$

bridges blocking counterion approach.

12. Discussion: Rotational Barrier. With such a high rotational barrier as was observed for $\mathbf{1}^+$ rotation, and the possibility of electron-transfer catalysis, how confident we can be that the observed $\mathbf{1s}^+$ to $\mathbf{1a}^+$ isomerization rate really reflects simple thermal rotation about the NN bond must be addressed. There are several ways to get too low of a barrier, and none we can think of to get too high of a barrier. Adventitious impurities certainly do cause more rapid isomerization, and we found that neither purification of the solvent by distillation from calcium hydride nor by filtration through alumina gave reproducible isomerziation data. Distillation from phosphorus pentoxide did give slower isomerization rates, with excellent reproducibility from batch to batch of $\mathbf{1}^+PF_6$ and in different months. In the electron-transfer-catalyzed isomerization work, it was found that addition of 1.2×10^{-6} M neutral **1** to a sample of $\mathbf{1}^+$ (0.2% as much $\mathbf{1}^0$ as $\mathbf{1}^+$) increased k_{obsd} by a factor of 11. Electron-transfer isomerization is second order, and obtaining the same rate constants for the factor of four concentration difference between the CV and UV experiments is additional evidence that the rate constants of Table I do not just reflect adventitious impurities.

An electron-transfer pathway for isomerizing $\mathbf{s1}^+$ to $\mathbf{a1}^+$ without impurities present would be by disproportionation followed by other electron transfers as indicated in Scheme III. Although the first step is over 20 kcal/mol endothermic, the second step is slightly exothermic. Since it has a barrier of 12.3 kcal/mol, which will be added to the thermodynamic barrier for the first step, this pathway cannot be rapid enough to account for the isomerization observed. Step 1 followed by step 3 does not seem as easily ruled out. We know nothing about the barrier for $\mathbf{1}^{2+}$, $\mathbf{1}^+$ electron transfer, and it might be much lower than the $\mathbf{1}^0$, $\mathbf{1}^+$ barrier (the NN bond shortening involved in loss of a second electron is estimated by MNDO to be on the order of half as large as that involved in the first electron, and essentially no barrier due to flattening at N should be present for the $\mathbf{1}^{2+}$, $\mathbf{1}^+$ electron transfer).

It is of interest to compare the observed k_1 for $\mathbf{1}^+$ with that estimated by MO calculations. Reasonably accurate calculations can only be done at present for the smallest compounds. We found a small increase in the calculated rotational barrier for $H_4N_2^+$ as the level of ab initio calculation was increased: 3-21G, 28.6; 6-31G*, 28.8; MP2-6-31G*, 30.2 kcal/mol. We predict that alkyl substitution will lower the barrier because charge becomes localized on one nitrogen at the transition state (see below) and because the ground state will be more destabilized by *RN*, N'*R* interactions. The $\Delta G^\ddagger$ observed for $\mathbf{1}^+$ isomer interconversion seems quite in line with what might be expected from MO calculations on $H_4N_2^+$.

Calculations at all levels, including MNDO, predict that the nitrogens of $H_4N_2^+$ become very different at the transition state for NN bond rotation. One N remains flat, but the other bends past tetrahedral, causing the charge to localize on the flat nitrogen because its half-filled orbital has pure p character. The MNDO-calculated rotational barrier for $H_4N_2^+$ is 26.7 kcal/mol, or 88% that of the highest level calculation. We thought it worthwhile to see what MNDO calculates the barrier shape to be like; it is prohibitively time-consuming to investigate such a question at a much higher level of calculations. Although MNDO gets the equilibrium $H_4N_2^+$ geometry to be slightly anti-bent, presumably incorrectly because higher level ab initio calculations make it planar, the energy involved is not great, as is seen in the energy plot of Figure 13. Allowing the nitrogens to be different starts to significantly affect the energy at twist angles of greater than 70° and less than 110°, i.e., when the three-electron π bond has been almost completely broken. At 90° twist, requiring both nitrogens to be bent the same amount costs 7.7 kcal/mol, and

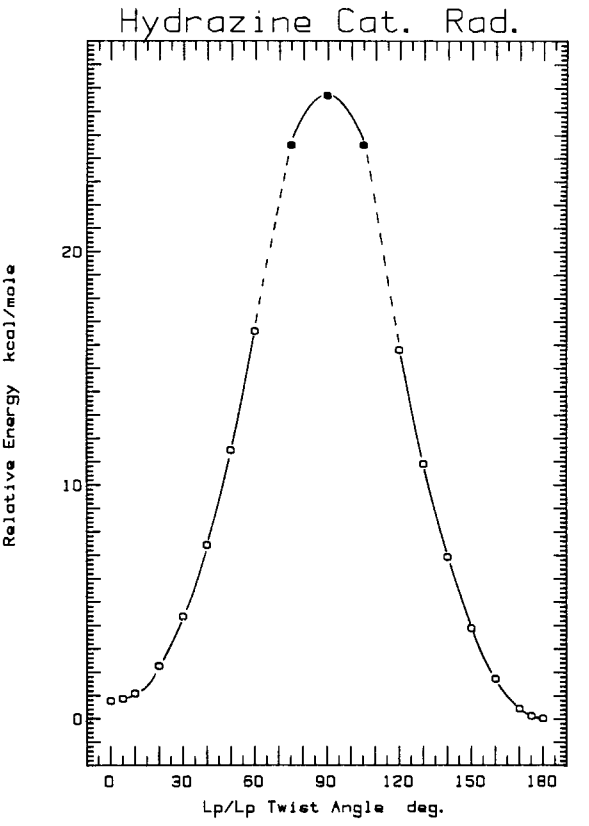

Figure 13. MNDO-UHF calculated barrier for $H_4N_2^+$ rotation about the NN bond. Open circles, nitrogens equivalent. Filled circles, nitrogens allowed to be different.

requiring them both to be planar costs 12.9 kcal/mol relative to the minimum energy 90° conformation shown (one N flat, the other with β(NN) 15.5°, d(NN) = 1.36 Å). As might be expected, the first 20° twist costs little energy (1.7 kcal/mol), but the energy curve increases sharply, and 30° twist from coplanar lone pair orbital axes costs 3.9 kcal/mol.

Although nitrogen very clearly stabilizes radical centers α to it, and many of the very stable radicals such as hydrazyls, nitroxides, and hydrazine radical cations share such three-electron π bond stabilization, few experimental results quantitating the stabilization available have appeared. Möbius and co-workers[21] estimated the NN rotational barrier of 1-picryl-2,2-diphenylhydrazyl to be between 9 and 12 kcal/mol, since the rotation rate was too fast to measure on the NMR time scale and too slow to measured by ESR. Balaban and co-workers[22] adjusted substituents to obtain a measurable barrier for 1-benzoyl-2,2-bis(3,5-di-*tert*-butylphenyl)hydrazyl, obtaining 7.4 kcal/mol by VT-ESR. The stabilizing effect of the adjacent nitrogen on the radical center is obscured in these examples both by rather larger steric effects and by their three-electron π bonds being conjugated with both electron-donating and electron-withdrawing groups.

We earlier tried to estimate the stabilization provided by an α nitrogen to an amine radical cation by examining changes in $E^{\circ\prime}$ values for various R_2NX systems as a function of X group, employing a very crude method of accounting for inductive differences by using σ_I values.[4b] This procedure gave an estimated stabilization for 9-azabicyclo[3.3.1]nonane radical cation substituted with a 9-(dimethylamino) group of 19 kcal/mol and was asserted to be a way of estimating the rotational barrier for a tetraalkylhydrazine radical cation. The rotational barriers measured in this work are rather close to this estimate, quite possibly by accident.

(21) Möbius, K.; Biehl, R.; O'Connor, S. E.; Walter, R. I.; Zimmerman, H. *J. Phys. Chem.* **1979**, *83*, 3449.

(22) Balaban, A. T.; Caproiu, M. T.; Elian, M.; Grecu, N.; Negoita, N. *J. Chem. Soc., Perkin Trans. 2* **1983**, 591.

Lossing and Griller[23] have derived stabilization energies for simple nonconjugated α-amino radicals from the appearance energies for fragmentation of a series of ethylenediamine derivatives. The appearance energy, AE, is the energy required for an electron beam to produce a detectable amount of $R_2NCH_2^+$ ion in the mass spectrometer and is related to ΔH_f of the radical by the relationship

$$R_1 - R_2 + e \xrightarrow{AE} R_1^+ + R_2 + 2e$$

$$AE = \Delta H_f(R_1^+) + \Delta H_f(R_2) - \Delta H_f(R_1 - R_2)$$

By using established values for ΔH_f of R_1^+ and R_1R_2, $\Delta H_f(R_2\cdot)$ was evaluated, and stabilization energies for the α-amino radicals were estimated, giving 10 kcal/mol for NH_2 and 20 kcal/mol for NMe_2. They therefore find experimentally as much stabilization by NMe_2 for a carbon-centered radical in the gas phase as we estimated for a nitrogen-centered radical cation in solution from $E^{\circ\prime}$ value changes and measured experimentally for the rotational barrier in $\mathbf{1}^+$ (assuming that this barrier is reasonably related to "stabilization", since the NN π bond must be broken for rotation to occur). We find the size of the NMe_2 stabilization of a neutral carbon radical surprisingly large, because we would have expected a larger effect of the inherent energy of the two orbitals involved upon the stabilization energy. We would have thought that the symmetrical $R_4N_2^+$ ought to show substantially more stabilization than the unsymmetrical $R_4NC\cdot$ case. The phase change between the two types of experiments might prove significant. Estimation of stabilization in $R_4NC\cdot$ by the $E^{\circ\prime}$ change method is difficult for several reasons, not the least because only a difference in stabilization between R_4NC^+ and $R_4NC\cdot$ can be obtained, and the former is not really known experimentally, but a much smaller stabilization than 20 kcal/mol for the latter seemed to be indicated.[4b]

13. Discussion: Homogeneous $\mathbf{1}^0$, $\mathbf{1}^+$ Electron-Transfer Barrier. Although it has been clear for several years from a variety of experiments (heterogeneous electron-transfer rates, internal electron-transfer rates in hexahydrotetrazines, lack of NMR line broadening in a derivative of **2**)[2] that homogeneous electron transfer between hydrazine and their cation radicals is unusually slow, the work reported above is the first quantitative measure of a k_2 value. The "intrinsic barrier" (the average of $\Delta G^{\ddagger}_2$ and $\Delta G^{\ddagger}_{-2}$, 13.1_5 kcal/mol, estimating the barrier if electron transfer were thermoneutral) corresponds to a rate constant of 1.1×10^3 M^{-1} s^{-1} at 22 °C. This is on the order of 10^6 slower than the rate of electron exchange for *N,N,N′,N′*-tetramethyl-*p*-phenylenediamine and its cation radical of 1.05×10^9 M^{-1} s^{-1} or anthracene radical anion, anthracene of 2.4×10^8 M^{-1} s^{-1}.[24] The "classical" case of a slow electron transfer is that between cyclooctatetraene and its radical anion, which is unquestionably slower than that between the radical anion and the dianion.[25] This slowness has usually been attributed to the large conformational change (tub with alternate bond lengths to almost planar with equal bond lengths) which accompanies electron transfer. The rate of electron transfer here, as in other cases,[24] is clearly very sensitive to counterion and solvent polarity effects. It seems valid to conclude[25,26] that the contribution of the structrual change to the sluggishness of COT reduction was probably overemphasized in the earlier work. The slow value for **1**, $\mathbf{1}^+$ homogeneous electron transfer reported here was determined in a good ionizing solvent, CH_3CN, with perchlorate counterion, at room temperature, and observing an intrinsic barrier some 7 orders of magnitude below diffusion control can most reasonably be attributed to the large geometry change which accompanies electron transfer. The basic tenet of the Marcus theory of electron-transfer reactions[24] is that electron transfer is much faster than any nuclear motion, so that when a large solvation or geometry change results from electron transfer, the inherent barrier is caused by the energy necessary to make the reactants isogeometric with the products. The geometry change between $\mathbf{1}^0$ and $\mathbf{1}^+$ is unusually well documented and has been shown to involve both extreme flattening at the nitrogens and an NN bond length shortening of about 10%.

Conclusion

In retrospect, we could not have devised better properties for *syn*- and *anti*-$\mathbf{1}^+$ and -$\mathbf{1}^{2+}$ for the purposes of this work if we had been allowed to choose them individually. A 1.5 kcal/mol difference in stability of the $\mathbf{1}^+$ isomers is just right for being able to measure ΔG° yet having their equilibration go almost to completion. The turnaround in stability at the dication stage provides a big enough $\Delta E^{0\prime}$ to allow quantitative measurement of the isomer ratio. The 19-nm λ_m shift between the isomeric radical cations provides both the way to form a nonequilibrium mixture favoring the minor isomer and a means of following the isomerization. All these properties were, of course, quite unpredicted, although previous work[4] had shown that both the radical cation and dication of **1** should be long-lived, which is also necessary for the experiments to work. These properties allowed the first reliable measurement of a $R_4N_2^+$ rotational barrier and of a $R_4N_2^+$, R_4N_2 electron-transfer rate constant, two quantities we have been fumbling to measure property for years. It will be particularly important to probe the questions of how changes in steric hindrance and relative amounts of geometry change affect these quantities. This can only be accomplished by changing alkyl group structure and the indentity of the heteroatoms. It remains to be seen if other R_4N_2 examples or other three-electron π bond systems will prove to be similarly convenient to study.

Experimental Section

8-Chloro-8-azabicyclo[3.2.1]octane (5) was prepared by exactly the same sequence of steps as previously reported for the bicyclononane derivative,[3] using the Robinson–Schöpf condensation conditions of Shimizu and Uchimaru[26] to prepare 8-methyl-8-azabicyclo[3.2.1]octan-3-one in 83% yield after two sublimations at 50–60 °C (1–2 torr). The Wolff–Kishner reduction went in 71% yield, phenyl carbamate formation in 90% yield, and hydrolysis to 8-azabicyclooctane hydrochloride in 85% yield. Crude 8-aza-bicyclooctane hydrochloride (2.48 g) gave 1.73 g (71%) of crude 8-chloro-8-azabicyclo[3.2.1]octane as an oil, which was purified by column chromatography (silica, 15% ethyl acetate in hexane) to give 1.27 g (52%) as a colorless oil. Empirical formula $C_7H_{12}NCl$ was established by high-resolution mass spectroscopy: ^1H NMR ($CDCl_3$) δ 3.62 (br s, 2 H), 2.42–2.18 (m, 2 H), 2.1–1.2 (m, 10 H); ^{13}C NMR ($CDCl_3$) 70.1 (CH), 33.4 (CH_2), 26.3 (CH_2), 14.5 (CH_2).

8,8′-Bi(8-azabicyclo[3.2.1]octane), 1, was made from 0.5 g of **5** by the procedure previously reported for **2**.[3] The pale-orange crude product was sublimed (50–55 °C, 0.2 torr) to give 0.28 (74%) of **1** as a white solid, mp 77–78 °C. Empirical formula $C_{14}H_{22}N_2$ was established by high-resolution mass spectroscopy: ^1H NMR ($CDCl_3$) δ 3.39 (br s, 4 H), 1.97 (m, 4 H), 1.83 (m, 4 H), 1.55–1.10 (m, 8 H), 1.25 (m, 4 H); ^{13}C NMR reported in text.

8,8′-Bi(8-azabicyclo[3.2.1]octenium) Hexafluorophosphate, $\mathbf{1}^+PF_6^-$. A solution of 51.4 mg of $NOPF_6$ in 10 mL of methylene chloride was added to 64.5 mg of **1** in 10 mL of methylene chloride at −78 °C, and after 1 h the solution was allowed to come to room temperature and stirred an additional 2 h. Solvent removal gave 0.11 g of yellow solid, which was recrystallized from acetone. Heating above 220 °C causes obvious decomposition.

Anal.[27] Calcd for $C_{14}H_{24}F_6N_2P$: C, 46.03; H, 6.62; N, 7.67. Found: C, 45.94; H, 6.58; N, 7.54%.

8,8′-Bi(8-azabicyclo[3.2.1]octenium Nitrate, $\mathbf{1}^+NO_3^-\cdot H_2O$. A 0 °C solution of 46.6 mg (0.21 mmol) of **1** in 15 mL of acetone was treated with 36.0 mg (0.21 mmol) of $AgNO_3$ in one portion. The mixture was stirred 3 h at 0 °C while a gray precipitate (silver) formed and the solution turned yellow. Filtration through a Celite plug and solvent removal gave 46 mg (78%) of $\mathbf{1}^+NO_3^-$, which was recrystallized from 4:1

(23) (a) Lossing, F. P.; Griller, D. *J. Am. Chem. Soc.* **1981**, *103*, 1586. (b) Lossing, F. P.; Burkey, T. J.; Castelhano, A. L.; Griller, D. *Ibid.* **1983**, *105*, 4701.

(24) For excellent reviews of organic electron-transfer reactions, see: (a) Szwarc, M.; Jagur-Grodzinski, J. "Ions and Ion Pairs in Organic Reactions"; Szwarc, M., Ed.; Wiley: New York, 1974; pp 1–150. (b) Eberson, L. *Adv. Phys. Org. Chem.* **1982**, *18*, 79–185.

(25) For a review of COT reduction and related cases, see section V of: Evans, D. H.; O'Connell, K. M. "Electroanalytical Chemistry"; Bard, A. J., Ed.; Marcel Dekker: New York, in press.

(26) Jensen, B. J.; Ronlan, A.; Parker, V. D. *Acta Chem. Scand., Ser. B* **1975**, *29*, 394. Shimizu, M.; Uchimaru, F. *Chem. Pharm. Bull.* **1961**, *9*, 300; *Chem. Abstr.* **1962**, *56*, 10092*i*.

(27) Spang Microanalytical Laboratory, Eagle Harbor, MI.

Table VI. Summary of Crystal Data and Intensity Collection

parameter	1	$1^+NO_3^-\cdot H_2O$
emperical form	$C_{14}H_{24}N_2$	$C_{14}H_{26}N_3O_4$
formula wt	220.36	318.39
temp, K	293	198 ± 5
cell parameters		
a, Å	10.698 (6)	12.889 (3)
b, Å	9.204 (5)	10.521 (5)
c, Å	12.438 (6)	6.514 (2)
β, deg		114.06 (1)
space group	*Pbca*	*C2/m*
Z	4	2
density calcd, g/cm^3	1.20	1.31
absorpt coeff μ, cm^{-1}	0.36	0.61
2ϑ limits, deg	5.0–50.0	3.5–60.4
sin θ/λ_{max}, Å^{-1}	0.595	0.708
unique data, theoret	1063	1198
used in refinement	1063	863
discrepency index		
R_1	0.064	0.063
R_2	0.098	0.067
goodness of fit		1.71

toluene/acetone. Decomposition occurs above 195 °C.

Crystallography for 1. Single crystals were obtained by sublimation. Preliminary examination and collection of the diffraction data were carried out on a Phillips PW 1100 computer-controlled diffractometer. The X-ray intensity data were collected by using a ϑ–2ϑ scan technique with 1.20° scan widths and 24-s peak scan times. Stationary-crystal stationary-counter backgrounds were measured for 10 s at each end of the scan. Details of the intensity collection parameters and crystal data are given in Table VI. All measurements utilized monochromated Mo K_α radiation (λ = 0.71073 Å). The structure was solved by direct methods by using the MULTAN package[28] and refined by full-matrix least-squares techniques. Standard values for the atomic scattering factors were employed in the structure analysis.[29] Final R values are included in Table VI. Details of the structure are given in the supplementary material.

Crystallograph for 1^+. Crystals of $1^+NO_3^-\cdot H_2O$ were obtained by vapor diffusion of pentane into wet methhylene chloride at −15 °C. A single crystal of dimensions 0.15 × 0.22 × 0.70 mm was mounted on a glass filter and coated with cyanoacrylate glue for the X-ray study. All measurements were examined on a Synthex-Nicolet P1 diffractometer equipped with a modified T-1 low-temperature device. The data were collected by using an ω step scan technique with a scan width of 0.15° in ω centered on 2θ MoK_α^-, and variable scan rate (0.5–12.0°/min) stationary-crystal stationary-counter backgrounds were collected on both sides of the peak (offset 1.30° from the peak center), each for 25% of the total scan time. Structure amplitudes and their standard deviations were calculated from intensity data by procedures similar to those described previously.[30] Crystal data are given in Table VI. All measurements utilized monochromated Mo Kα radiation (λ = 0.71069 Å), and the structure was solved by direct methods by using the MULTAN package.[28] Standard values for the atomic scattering factors were employed in the structure analysis.[29] After preliminary refinement, the position of the solvent water molecule was determined in an electron density difference map. Subsequent electron density difference maps revealed the positions of all the hydrogen atoms. In the final models, all non-hydrogen atoms were assumed to vibrate anisotropically. The hydrogen atoms were assumed to vibrate isotropically and their positioned and thermal parameters were included in the refined variables. Final R values are included in Table VI. The details of the structure are given in the supplementary material.

ENDOR spectra of 1^+ were recorded on a Brucker ER220D ESR spectrometer equipped with a Brucker cavity (ER 200 ENB) and NMR facilities described elsewhere.[31]

Cyclic voltammetry was performed with a Princeton Applied Research (PAR) 173 potentiostate equipped with a PAR 176 current-to-voltage converter, and the voltage ramp was generated by a PAR 175 universal programmer. CV data were acquired and stored with a nicolet Explorer III digital oscilloscope, stored on magnetic minidisks by a Commadore PET 2001 microcomputer, and analyzed as previously described.[32] Temperature in the jacketed cell[32] was controlled with a Lauda K-2/R circulating bath and measured with a Doric 410A digital thermometer by using an iron–constantan couple. Temperature was constant to ±0.1 °C. The electrode has been previously described.[33] The background-corrected digitized data were transferred to the Harris computer, converted to laboratory units (mA vs. V) and smoothed by using program CVSMOOTH. Fitting used the direct simulation method.[34] An Ag/Ag^+ (0.01 M $AgNO_3$ in CH_3CN) reference electrode was employed because it remained stable during long kinetic runs. Acetonitrile (Burdick & Jackson distilled in glass) was freshly distilled from phosphorus pentoxide, and sample solutions were 2–3 mM in $1^+PF_6^-$ and 0.14 M in tetrabutylammonium perchlorate (Eastman, twice recrystallized from 1:1 H_2O/EtOH). The sample solutions were deoxygenated with a stream of nitrogen and allowed to thermally equilibrate before acquiring the initial voltammogram. Isomerization to a nonequilibrium 1^+ isomer mixture was accomplished by irradiation with a 275-W Sylvania sunlamp while a stream of nitrogen bubbled through the sample. The extent of isomerization was monitored by CV and took 60–100 s. After irradiation, the cell was protected from light and allowed to thermally equilibrate (typically, 5 min). The solvent/electrolyte contribution to the measured current was subtracted from the experimental data by a point-by-point subtraction of signal from a blank solution. The simulated model for the $\mathbf{a1}^+$, $\mathbf{s1}^+$ CV analysis consists of two noninterconverting species which are oxidized at different potentials. The ratio of the two was adjusted until a good fit with experimental data was achieved. Complete details on the more complex kinetic schemes appear in the thesis.[35] The first wave simulations employed data from a gold electrode, where electron transfer is faster, but the second wave work was done at platinum.

UV kinetic experiments used a Cary 118 spectrophotometer equipped with a VT cell holder, the temperature being controlled with a Lauda K-2/R circulating bath, and the temperature was measured with a thermocouple immersed in the reference cell. When the temperature stopped drifting, the thermocouple wire was removed. Temperature measurement after completion of the kinetic run invaraibly gave the same reading to ±0.05 °C. The samples were 6–7 × 10^{-4} M in $1^+PF_6^-$ and 0.14 M in TBAP. Isomerization was accomplished by irradiation of the sample at 366 nm while it was still in the thermostated cell holder, using a Orsam sp 200 mercury lamp and Bausch & Lomb short path monochrometer until the absorption at 360 nm had decreased about 0.1 unit. The sample was quickly removed and shaken before the kinetic run was started.

Rate Constants. The value of k_{obsd} was determined by least-squares analysis of the ln $([\mathbf{1a}^+_{eq}]/[\mathbf{1a}^+_{eq}] - [\mathbf{1a}^+])$ vs. time plot for the CV data and absorption vs. time for the UV data, using program CONINFIN.[20] First-order plots for the data of Table I appear in the thesis.[19]

Acknowledgment. We thank the National Science Foundation for partial financial support of this work under Grant CHE-8026111 (S.F.N.) and NATO for a travel grant (D.104/80) which allowed the extensive collaboration represented in this work to occur. We thank Silas C. Blackstock for assistance with some MNDO calculations. H. K. thanks the Deutsche Forschungsgemeinschaft and the Fonds der Chemischen Industrie for financial support. B. K. gratefully acknowledges a Liebig stipend of the Fonds der Chemischen Industrie.

Registry No. 1, 56847-10-0; $1^+\cdot PF_6^-$, 86782-27-6; $1^+\cdot NO_3^-\cdot H_2O$, 96258-24-1; *syn*-$1^{2+}$, 96258-25-2.

Supplementary Material Available: Stereoscopic view of the crystal packing of **1** and $1^+NO_3^-\cdot H_2O$, tables of bond length, angles, dihedral angles, fractional coordinates, isotropic and anisotropic thermal parameters, and observed and calculated structure factors for **1** and $1^+NO_3^-\cdot H_2$, Figures 10–12, and comparison of experimental with simulated CV curves for **1** at 22 °C (34 pages). Ordering information given on any current masthead page.

(28) Germain, G.; Main, P.; Woolfson, M. N. *Acta Crystallogr., Sect. A* **1971**, *27A*, 368.
(29) Atomic form factors were from: Cromer, D. T.; Mann, J. B. "International Tables for X-ray Crystallography"; Kynoch Press: Birmingham, England, 1974, Vol. 4, p 99, Table 2.2 B. The atomic form factor for hydrogen was from: Stewart, R. F.; Davidson, E. R.; Simpson, W. T. *J. Chem. Phys.* **1965**, *42*, 3175.
(30) Haller, K. J.; Enemart, J. H. *Inorg. Chem.* **1978**, *17*, 3552.
(31) Kurreck, H.; Kirste, B.; Lubitz, W. *Angew. Chem., Int. Ed. Engl.* **1984**, *23*, 273.
(32) O'Connell, K. M.; Evans, D. H. *J. Am. Chem. Soc.* **1983**, *105*, 1473.
(33) Nelsen, S. F.; Echegoyen, L.; Clennan, E. L.; Evans, D. H.; Corrigna, D. A. *J. Am. Chem. Soc.* **1977**, *99*, 1130.
(34) Feldberg, S. In "Electroanalytical Chemistry"; Bard, A. J., Ed.; Marcel Dekker: New York, 1969; Vol. 3, pp 199–295.
(35) Cunkle, G. T. Ph.D. Thesis, University of Wisconsin, 1984.
(36) Written by John J. Houser, University of Akron, Akron, OH.